CHAPTER 4

Moment Invariants for Image Symmetry Estimation and Detection

Miroslaw Pawlak

We give a general framework of statistical aspects of the problem of understanding and a description of image symmetries, by utilizing the theory of moment invariants. In particular, we examine the issues of joint symmetry estimation and detection. These questions are formulated as the statistical decision and estimation problems since we cope with images observed in the presence of noise. The estimation/detection procedures are based on the minimum L_2-distance between the reconstructed image function and the reconstruction of its hypothesized symmetrical version. Our reconstruction algorithms are relying on a class of radial orthogonal moments. The proposed symmetry estimation and detection techniques reveal some statistical optimality properties. Our technical developments are based on the statistical theory of nonparametric testing and semi-parametric inference.

Miroslaw Pawlak
Electrical and Computer Engineering, University of Manitoba
Winnipeg, Canada
e-mail: Miroslaw.Pawlak@umanitoba.ca

Editor: G.A. Papakostas, *Moments and Moment Invariants - Theory and Applications*
DOI: 10.15579/gcsr.vol1.ch4, GCSR Vol. 1, ©Science Gate Publishing 2014

4.1 Introduction

Symmetry plays an important role in signal and image understanding, compression, recognition and human perception [18]. In fact, symmetric patterns are common in nature and in man-made objects thus estimation and detection of image symmetries can be useful for designing efficient algorithms for object recognition, robotic manipulation, image animation, and image compression [11]. Though symmetry can be discussed from different point of views, in this chapter statistical aspects of spatial symmetry are examined and reviewed. We are aiming at the fundamental problems of estimating symmetry parameters like the angle of the axis of mirror symmetry and detection of symmetry type.
For objects represented by a function f that belongs to the space $\mathcal{F}$ one can define a symmetry class on $\mathcal{F}$ as follows

$$\mathcal{S} = \{f \in \mathcal{F} : f = \tau_\theta f, \theta \in \Theta\}, \tag{4.1}$$

where τ_θ is mapping $\tau_\theta : \mathcal{F} \to \mathcal{F}$ that represents the transformed version of f. The mapping τ_θ is parametrized by $\theta \in \Theta$, where typically Θ is a compact subset of R^p. Hence, the class $\mathcal{S}$ is a subset of $\mathcal{F}$ defining all objects from $\mathcal{F}$ that are symmetric with respect to the class of operations $\{\tau_\theta\}$ parametrized by $\theta \in \Theta$.

In the concrete situation of image analysis an object f is identified with the grey-level bivariate image function $f(x, y)$. In this case there are two basic symmetry types, i.e., mirror (reflection) and rotational symmetries. In the former case there is an axis of symmetry that divides the image into two identical reflected images. Formally, the image reveals the mirror symmetry if it belongs to the following class

$$\mathcal{S}^m = \{f \in \mathcal{F} : f(x, y) = \tau_\theta^m f(x, y), \theta \in \Theta\}, \tag{4.2}$$

where

$$\tau_\theta^m f(x, y) = f(x\cos(2\theta) + y\sin(2\theta), x\sin(2\theta) - y\cos(2\theta))$$

is the reflection of the image $f(x, y)$ with respect to the axis of symmetry defined by the angle $\theta \in \Theta \subset [0, \pi)$. In rotation symmetry there is a single rotation point such that the image rotated about this point by a fraction (degree) of a full cycle aligns with the original image. The corresponding rotation symmetry class $\mathcal{S}^r$ is defined as in (4.2) with the rotation transformation through the angle θ defined as

$$\tau_\theta^r f(x, y) = f(x\cos(\theta) + y\sin(\theta), -x\sin(\theta) + y\cos(\theta)).$$

The rotation angle θ takes commonly the form $\theta = 2\pi/d$, where d is an integer called the rotation degree and the corresponding class $\mathcal{S}^r$ is referred to as the d-fold rotation symmetry class.

It is also convenient to express the above symmetry constrains in terms of polar coordinates. Hence, let $f(\rho, \varphi)$ be the version of the image function in polar coordinates. Then, the mapping in (4.2) is given by

$$\tau_\theta^m f(\rho, \varphi) = f(\rho, 2\theta - \varphi) \tag{4.3}$$

with the corresponding symmetry requirement $f(\rho, \varphi) = f(\rho, 2\theta - \varphi)$ for some angle θ. Common mirror symmetry classes are: vertical symmetry ($\theta = \pi/2$), horizontal

symmetry ($\theta = 0$), and diagonal symmetry ($\theta = \pi/4$). Analogously, the d-fold rotation class in polar coordinates is defined by the mapping

$$\tau_\theta^r f(\rho, \varphi) = f(\rho, \varphi - 2\pi/d) \tag{4.4}$$

and the corresponding symmetry requirement $f(\rho, \varphi) = f(\rho, \varphi - 2\pi/d)$ for some degree d. There are a few important values of d: $d = 2$ gives the rotation class by π, $d = 4$ defines the rotation class by $\pi/2$. The limit value $d = \infty$ corresponds to radial images, i.e., when $f(\rho, \varphi) = g(\rho)$ is a function of the radius ρ only for some univariate function g.

The aforementioned transformations can be combined to define joint symmetries. For example, one can consider a joint symmetry with respect to the horizontal and vertical transformations. We can easily verify that $\tau_{\pi/2}^m \tau_0^m f = \tau_\pi^r f$ and $\tau_\pi^r \tau_{\pi/2}^m f = \tau_0^m f$. Hence, the symmetry group generated by $\{\tau_0^m, \tau_{\pi/2}^m\}$ is identical to that generated by $\{\tau_{\pi/2}^m, \tau_\pi^r\}$. Thus, one can consider the symmetry class generated jointly by the vertical reflection $\tau_{\pi/2}^m$ and the 2-fold rotation τ_π^r. Generally, a symmetry group generated by two reflections can always be generated by a reflection and a rotation.

In real-world applications we do not have a complete information about the image function f and one must verify the question whether f reveals some type of symmetry observing only its discrete and noisy version. In fact, in image processing systems one needs to address the following fundamental issues:

1. Detection of the type of symmetry present in the original unobserved image.
2. Estimating the parameters characterizing the given type of symmetry, i.e., the angle of mirror symmetry and the degree of rotational symmetry.

Moreover, we need to estimate the location of symmetry axis and the point of rotation. These problems, however, can be easily resolved by a proper image normalization. Throughout this chapter, we assume that these points are located in the coordinate system origin being the image center of inertia.

In this chapter, we assume that the only information we have about the original image function is its noisy and digitized version. Hence, suppose we have discrete noisy image data observed over the region D

$$Z_{i,j} = f(x_i, y_j) + \varepsilon_{i,j}, \quad (x_i, y_j) \in D, \quad 1 \le i, j \le n, \tag{4.5}$$

where the noise process $\{\varepsilon_{i,j}\}$ is a random sequence with zero mean and finite variance σ_ε^2. The data are observed on a symmetric square grid of edge width Δ, i.e., $x_i - x_{i-1} = y_i - y_{i-1} = \Delta$ and (x_i, y_j) is the center of the pixel (i, j). Note that Δ is of order $1/n$ and the image size is n^2.

We may believe that hidden in the noisy data $\{Z_{i,j}, 1 \le i, j \le n\}$ our image exhibits the one of the aforementioned symmetry type τ_{θ_0} for some $\theta_0 \in \Theta$. Thus, we wish to detect the symmetry type τ and estimate the corresponding true symmetry parameter θ_0 from $\{Z_{i,j}, 1 \le i, j \le n\}$. The statistical nature of the observed image data and the lack of any a priori knowledge of the shape of the underlying image $f(x, y)$ call for formal nonparametric statistical methods for joint estimating and testing the existing symmetry in an image function.

To appreciate the difficulty of the posed problem we display in Fig.(4.1) the discrete and noisy image that represents the true mirror symmetric image $f(x,y)$ (shown on the left-hand-side) observed over the rectangular region with the resolution $n \times n = 30 \times 30$. The problem of detection and estimation of the existing symmetry in $f(x,y)$ based merely on $\{Z_{i,j}\}$ is clearly challenging.

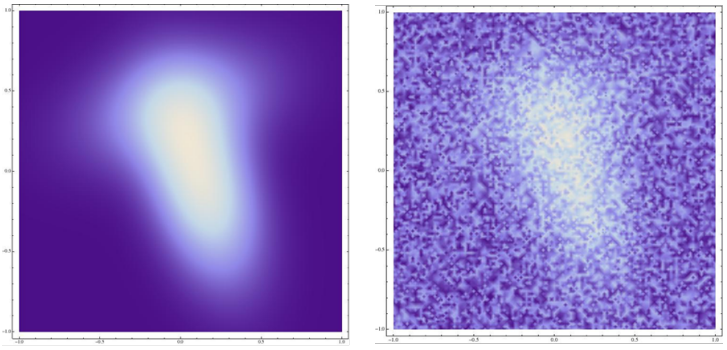

(a) (b)

Figure 4.1: (a) The original mirror symmetric image $f(x,y)$. (b) The discrete and noisy version $\{Z_{i,j}\}$ of the image in (a).

Some preliminary studies examining statistical aspects of symmetry estimation and detection have been initiated in [2, 3, 4, 16]. In this chapter, we propose a systematic and rigorous statistical approach for joint estimating and testing of the aforementioned image symmetries. To do so, we use the orthogonal moments image representation utilizing the theory of radial functions expansions [16, 20]. In particular, we select the specific radial basis commonly referred to as Zernike functions [1]. The Zernike functions define an orthogonal and rotationally invariant basis of radial functions on the unit disk. As such, the Zernike functions and their corresponding Fourier coefficients (moments) have been extensively used in pattern analysis [10, 17, 16, 20].

Our estimation and test statistics are constructed by expressing the symmetry condition in terms of restrictions on radial moments. The estimation procedure is based on minimizing over $\theta \in \Theta$ the L_2 distance between empirical versions of f and $\tau_\theta f$ defining the aforementioned symmetry classes. Hence, f and $\tau_\theta f$ are estimated using truncated radial series with empirically determined Fourier coefficients. The inherent symmetry property of radial moments results in a particularly simple procedure for estimating θ.

The aforementioned estimation problem is closely connected to the problem of symmetry detection based also on the concept of the L_2 minimum distance principle. Hence, we wish to verify the following null hypothesis

$$H_0 : f = \tau_{\theta_0} f \tag{4.6}$$

for some $\theta_0 \in \Theta$, against the alternative

$$H_a : f \neq \tau_\theta f \tag{4.7}$$

for all $\theta \in \Theta$, where τ_θ is one of the above discussed symmetry classes. For a such formulated symmetry testing problem we propose detection statistics for which we establish asymptotic distributions, both under the null hypothesis of symmetry as well as under fixed alternatives. These results allow us to construct practical tests for the lack of symmetry and evaluate the corresponding power. Our results model the performance of our estimates and tests on the grid which becomes increasingly fine, i.e., when $\Delta \to 0$.

The chapter is organized as follows. In Section 4.2 we introduce our basic mathematical tools for representing the image symmetries in terms of radial moments. Section 4.3 is dealing with the symmetry estimation problem, whereas Section 4.4 examines the issue of symmetry detection.

4.2 Radial Moments and Image Symmetries

The symmetry constrains introduced in the previous section are convenient to express in some transform domain where we can parametrize the symmetry concept and to form estimates for symmetry detection and recovery. Let us begin with the classical geometric moments of the so-called complex form (complex moments) [7, 15]. Hence, let

$$C_{pq}(f) = \iint_D z^p z^{*q} f(x,y) dx dy,$$

be the (p,q)-order complex moment of f, where $z = x + jy$ and $z^* = x - jy$ is the conjugate of z. In polar coordinates $C_{pq}(f)$ can be expressed as

$$C_{pq}(f) = \int_0^R \int_0^{2\pi} \rho^{p+q} e^{j(p-q)\varphi} f(\rho,\varphi) \rho d\rho d\varphi,$$

where R defines the range of the image domain D. Let us now express the symmetry conditions in terms of $C_{pq}(f)$. Owing to the above representation of $C_{pq}(f)$ in terms of polar coordinates and Eq.(4.3) we can readily obtain that the complex moment of the image reflected by the axis tilted by the angle θ takes the following form

$$C_{pq}(\tau_\theta^m f) = e^{j(p-q)2\theta} C_{pq}^*(f).$$

The mirror symmetry condition implies that we must have

$$e^{j(p-q)2\theta} C_{pq}^*(f) = C_{pq}(f). \tag{4.8}$$

This equation puts some constrains on the admissible set of $\{C_{pq}(f)\}$ for which Eq.(4.8) holds. In fact, we can readily derive that if $C_{pq}(f) \neq 0$ then Eq.(4.8) is equivalent to

$$\arg(C_{pq}(f)) = (p-q)\theta,$$

where $\arg(C_{pq}(f))$ is the phase of $C_{pq}(f)$. In particular, for the horizontal reflection this implies that $C_{pq}(f)$ must be real, whereas for the vertical reflection we must have that $\arg(C_{pq}(f)) = (p-q)\pi/2$. Analogously by making use of Eq.(4.4) the complex moment of the image rotated by the angle θ we obtain

$$C_{pq}(\tau_\theta^r f) = e^{j(p-q)\theta} C_{pq}(f).$$

This yields that for the image exhibiting the d-fold rotation symmetry we have

$$e^{j(p-q)2\pi/d} C_{pq}(f) = C_{pq}(f). \tag{4.9}$$

This equation holds if we either have the constrain that $(p-q)/d$ is an integer or that $C_{pq}(f) = 0$. All the aforementioned formulas reveal that the classical complex moments must meet some restrictive constrains on (p, q) in order to capture the symmetry property of the image. Moreover, complex moments are not orthogonal and as such they exhibit some information redundancy and inability to uniquely recover the image function from imprecise data as in the noise model defined in Eq.(4.5). There is also little known about the accuracy of computing $C_{pq}(f)$ from digital and noisy data.

The function space $\mathcal{F}$ representing all images can be selected as $L_2(D)$ - the space of square integrable functions defined on a compact subset D of R^2. This function class allows us to represent images in terms of the orthogonal expansions of radial functions. It is also important to use the representation that can easily incorporate symmetry properties of the image. In [1] it is shown that a basis that is invariant in form for any rotation of axes must be of the form

$$V_{pq}(x, y) = R_p(\rho) e^{jq\varphi}, \tag{4.10}$$

where the right-hand-side is expressed in polar coordinates (ρ, φ). Here, $R_p(\rho)$ is a radial orthogonal polynomial of degree p and q defines the angular order. There are various ways of selecting $R_p(\rho)$ and important examples are Fourier-Mellin, pseudo-Zernike and Zernike radial bases [7, 17, 16, 20]. Among the possible choices for $R_p(\rho)$ there is only one orthogonal set, the set of Zernike functions, for which $R_p(\rho) = R_{pq}(\rho)$ is the radial orthogonal polynomial of degree $p \geq |q|$ such that $p-|q|$ is even [1]. Hence, the Zernike polynomial $R_{pq}(\rho)$ has no powers of ρ lower than $|q|$. In this chapter, without loss of generality, we confine our derivations and results to the Zernike basis. Analogous discussion can be carried out to other radial orthogonal basis.

An image function $f \in L_2(D)$ can be represented by the Nth-term expansion with respect to the given radial basis $\{V_{pq}(x, y)\}$

$$f_N(x, y) = \sum_{p=0}^{N} \sum_{q=-p}^{p} \lambda_p^{-1} A_{pq}(f) V_{pq}(x, y), \tag{4.11}$$

where $\lambda_p = \|V_{pq}\|^2 = 2\pi \|R_{pq}\|^2$ is the normalizing constant and $\|\cdot\|$ denotes the L_2 norm. In the case of Zernike polynomials we have $\|R_{pq}\|^2 = 1/2(p+1)$ yielding $\lambda_p = \pi/(p+1)$. Furthermore, the summation in Eq.(4.11) is taken with respect to the admissible pairs (p, q), i.e., $p \geq |q|$ and $p - |q|$ is even. Moreover, the image domain D is the unit disk. Then, the radial Zernike moment $A_{pq}(f)$ of the image f is defined as follows

$$A_{pq}(f) = \iint_D f(x, y)\, V_{pq}^*(x, y)\, dx\, dy.$$

It is also very useful to express $A_{pq}(f)$ in polar coordinates

$$A_{pq}(f) = \int_0^{2\pi} \int_0^1 f(\rho, \varphi) e^{-jq\varphi}\, R_{pq}(\rho)\, \rho\, d\rho d\varphi. \tag{4.12}$$

For future developments we need an expression on the L_2 distance between two images that can be expressed in terms of Zernike moments. Recalling Parseval's formula we have

$$\|f-g\|^2 = \sum_{p=0}^{\infty} \lambda_p^{-1} \sum_{q=-p}^{p} |A_{pq}(f) - A_{pq}(g)|^2. \tag{4.13}$$

In the following we shall work with an estimated version of the Zernike moments, since the only knowledge about the image function f is given by the data set $\{Z_{i,j}\}$ generated according to the model in Eq.(4.5). Hence, consider the weights

$$w_{pq}(x_i, y_j) = \iint_{\Pi_{ij}} V_{pq}^*(x,y)\, dxdy, \tag{4.14}$$

where $\Pi_{ij} = \left[x_i - \frac{\Delta}{2}, x_i + \frac{\Delta}{2}\right] \times \left[y_j - \frac{\Delta}{2}, y_j + \frac{\Delta}{2}\right]$ denotes the pixel centered at (x_i, y_j). Consequently, the Zernike moment $A_{pq}(f)$ is estimated by

$$\widehat{A}_{pq} = \sum_{(x_i,y_j)\in D} w_{pq}(x_i, y_j) Z_{i,j}, \tag{4.15}$$

where the weights are given by Eq.(4.14). A simple approximation for $w_{pq}(x_i, y_j)$ is given by $\Delta^2 V_{pq}^*(x_i, y_j)$, see [10, 17, 16] for higher order approximation schemes. The estimate $\widehat{A}_{pq}$ is a consistent estimate of the true A_{pq}. In fact, the bias $E\{\widehat{A}_{pq}\} = A_{pq} + O(\Delta)$ for a large class of image functions, whereas the variance $Var\{\widehat{A}_{pq}\}$ is of order $\sigma_\varepsilon^2 \frac{\pi}{p+1}\Delta^2$. As a result, we have that $\widehat{A}_{pq}$ tends (in probability sense) to A_{pq} as $\Delta \to 0$. Hence, for high resolution images the invariant property of A_{pq} discussed below is approximately satisfied by $\widehat{A}_{pq}$. It is also worth mentioning that along the boundary of the disk, some pixels are included and some are excluded. When reconstructing f from $\{\widehat{A}_{pq}\}$ this gives rise to an additional error called geometric error. This will be quantified in our considerations by the factor $\gamma < 1.5$, see [10, 17, 16] for a discussion of this important problem.

As a result, an estimate of the image function $f(x, y)$ from $\{\widehat{A}_{pq}\}$ is given by

$$\widehat{f}_N(x,y) = \sum_{p=0}^{N} \sum_{q=-p}^{p} \lambda_p^{-1} \widehat{A}_{pq} V_{pq}(x,y), \tag{4.16}$$

where N is a smoothing parameter which determines the number of terms in the truncated Zernike series. It was shown in [10, 17, 16] that the mean integrated square reconstruction error $MISE(\widehat{f}_N) = E\iint_D |\widehat{f}_N(x,y) - f(x,y)|^2 dxdy$ satisfies the property

$$MISE(\widehat{f}_{N^*}) = O(\Delta^{2/3}) \tag{4.17}$$

provided that the truncation parameter N is selected optimally as $N^* = a\Delta^{-2/3}$ some constant a. Other choices of N leads to slower decay of the error as Δ gets smaller, i.e., when the image resolution increases.

The fundamental property of radial moments and Zernike moments in particular is the easiness to embed the basic symmetry transformations into the radial moment

formula in Eq.(4.12). In fact, recalling the symmetry mappings defined in Eq.(4.3) and Eq.(4.4) and the formula in Eq.(4.12) we can obtain the following relationships

$$A_{pq}(\tau_\theta^m f) = e^{-2jq\theta} A_{pq}^*(f) \tag{4.18}$$

and

$$A_{pq}(\tau_\theta^r f) = e^{-jq\theta} A_{pq}(f) \tag{4.19}$$

for mirror and rotation symmetry mappings, respectively. The symmetry conditions can be now easily expressed in terms of $A_{pq}(f)$. Hence, the image f exhibits the mirror symmetry if

$$e^{-2jq\theta} A_{pq}^*(f) = A_{pq}(f) \tag{4.20}$$

for some $\theta \in [0, \pi)$. Next, we say that the image f exhibits the d-fold rotation symmetry if

$$e^{-jq2\pi/d} A_{pq}(f) = A_{pq}(f) \tag{4.21}$$

for some integer d. The above formulas put some constrains on the admissible set of Zernike moments. Hence, Eq.(4.20) holds if $A_{pq}(f) \neq 0$ and moreover, we have

$$arg(A_{pq}(f)) = -q\theta. \tag{4.22}$$

In particular, this implies that the horizontal mirror symmetry takes place if $A_{pq}(f)$ is real. On the other hand, Eq.(4.21) is satisfied if q/d is an integer or if $A_{pq}(f) = 0$. The important difference between these restrictions and the ones established for complex moments is that the symmetry invariance conditions of radial moments influence only the angular order q defining the Zernike moments $\{A_{pq}(f)\}$. Furthermore, the orthogonality property of Zernike functions allows us to group moments such that we are able to uniquely characterize the symmetry conditions in Eq.(4.20) and Eq.(4.21) and in the same time to recover the image. The conditions for the symmetry uniqueness of $\{A_{pq}(f)\}$ is described in Theorem 1 below.

Our strategy for both symmetry estimation and detection begins with forming the expansion as in Eq.(4.11) for both the original image f and its version obtained by the symmetry mapping $\tau_\theta f$. These two representations are then compared by L_2 distance and then the use of Eq.(4.13) giving the following contrast function

$$M_N(\theta) = \|f_N - \tau_\theta f_N\|^2 = \sum_{p=0}^{N} \lambda_p^{-1} \sum_{q=-p}^{p} |A_{pq}(f) - A_{pq}(\tau_\theta f)|^2. \tag{4.23}$$

It is clear that if f is symmetric with respect to the unique value $\theta = \theta_0$ corresponding to the symmetry mapping $\tau_\theta f$ then we have that $M_N(\theta_0) = 0$ for all N. It is important to verify whether $M_N(\theta) = 0$ uniquely determines θ_0. The following theorem gives a positive answer to this question.

Theorem 1. *Let $f \in L_2(D)$ be symmetric with respect to unique θ_0 corresponding to the symmetry mapping $\tau_\theta f$. Then for sufficiently large N, θ_0 is the unique zero of $M_N(\theta)$ if $M_N(\theta)$ contains nonzero $A_{p_1,q_1}, \ldots, A_{p_r,q_r}$ such that $p_i \leq N$, $i = 1, \ldots, r$ and*

$$\gcd(q_1, \ldots, q_r) = 1, \tag{4.24}$$

where $\gcd(q_1, \ldots, q_r)$ *stands for the greatest common divisor of* q_k*'s.*

Proof: Let us sketch the proof of this theorem in the case of mirror symmetry, i.e., where the mapping in Eq.(4.18) takes place. Then note that for $\theta \in [0, \pi)$ we have

$$|A_{pq}(f) - A_{pq}(\tau_\theta^m f)|^2 = 2|A_{pq}(f)|^2 \left(1 - \cos(2r_{pq}(f) + 2q\theta)\right),$$

where $r_{pq}(f)$ is the phase of $A_{pq}(f)$. This characterizes the true value θ_0 as

$$r_{pq}(f) + q\theta_0 = l\pi \tag{4.25}$$

for any integer l and all q with $A_{pq} \neq 0$. Next for any such A_{pq} we recall that A_{pq} is invariant for any rotation by an angle $\phi = 2\pi/q$ and its integer multiples. Hence, for any integer $m > 1$ such that q divides m we also have that A_{pq} is invariant by rotation by $2\pi/m$. Therefore, the gcd of all q with $A_{pq} \neq 0$ must be equal one. Hence, suppose that

$$A_{p_1 q_1} \neq 0, \ldots, A_{p_r q_r} \neq 0$$

with $\gcd(q_1, \ldots, q_r) = 1$ and $p_i \leq N$, $i = 1, \ldots, r$. Then, there are integers $a_1, \ldots, a_r$ such that

$$a_1 q_1 + \ldots + a_r q_r = 1. \tag{4.26}$$

By Eq.(4.25), if $\bar{\theta}$ is a zero of $M_N(\theta)$, then

$$r_{p_i q_i}(f) + q_i \bar{\theta} = l_i l\pi \tag{4.27}$$

for some integer l_i, $i = 1, \ldots, r$. By this and Eq.(4.26) it follows that

$$\bar{\theta} = -\sum_{i=1}^{r} a_i r_{p_i q_i}(f) + \bar{l}\pi,$$

where $\bar{l} = \sum_{i=1}^{r} a_i l_i$. Hence, the zero of $M_N(\theta)$ is uniquely determined and must be equal to θ_0. The proof of Theorem 1 has been completed. □

Hence, in practice one has to choose N large enough such that the sum defining $M_N(\theta)$ contains nonzero A_{pq}'s for which the condition given in Theorem 1 on the angular repetition q holds. Figure 4.2 illustrates the result described in Theorem 1 for an image being mirror symmetric with respect to $\theta_0 = \pi$. The contrast function $M_N(\theta)$ is depicted utilizing the terms with $q_1 = 1, q_2 = 3$ and $q_1 = 3, q_2 = 9$. The unique global minimum of $M_N(\theta)$ at θ_0 in the former case is clearly seen. This is not the case in the latter case.

The contrast function defined in Eq.(4.23) cannot be evaluated since we can only use the estimated Zernike moments defined in Eq.(4.15). Hence, the empirical counterpart of $M_N(\theta)$ can be defined as follows

$$\widehat{M}_N(\theta) = \sum_{p=0}^{N} \lambda_p^{-1} \sum_{q=-p}^{p} |\widehat{A}_{pq}(f) - \widehat{A}_{pq}(\tau_\theta f)|^2. \tag{4.28}$$

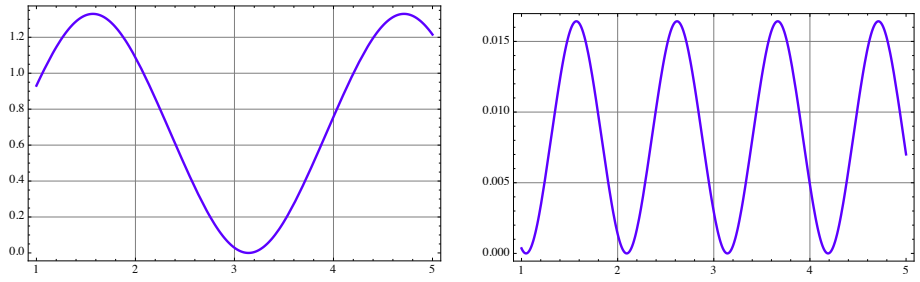

(a) (b)

Figure 4.2: (a) The true contrast function $M_N(\theta)$ utilizing the Zernike moments with $q_1 = 1, q_2 = 3$. (b) The true contrast function $M_N(\theta)$ utilizing the Zernike moments $q_1 = 3, q_2 = 9$.

This in the mirror symmetry case takes the following form

$$\widehat{M}_N(\theta) = \sum_{p=0}^{N} \lambda_p^{-1} \sum_{q=-p}^{p} |\widehat{A}_{pq} - e^{-2jq\theta} \widehat{A}^*_{pq}|^2, \tag{4.29}$$

where the summation in the above formula is taken with respect to those (p, q) that meet the conditions of Theorem 1. The estimate $\widehat{A}_{pq}$ is defined in Eq.(4.15) and $\widehat{A}^*_{pq}$ is its conjugate version. We show in this chapter that even for noisy images we need to estimate a few Zernike moments to properly identify symmetry parameters.

A number of ad hoc algorithms have been proposed for automatic estimation, detection and classification of image symmetries [6, 8, 9, 12, 13, 14]. The comprehensive summary of these methods is given in [11]. Most of the known symmetry detectors assume the access to clean images and they utilize the image variability extracted from the derivative of the image function. To our best knowledge there has not been a rigorous theory conducted for symmetry estimation and detection from noisy and discrete data.

4.3 Symmetry Estimation

Our approach to symmetry estimation is based on the minimum distance principle utilizing the L_2 distance expressed in terms of Zernike moments. Hence, due to Parseval's formula this is represented by the score function in Eq.(4.28) for the particular symmetry class τ_θ. Specialized this to the mirror symmetry we should take $\widehat{M}_N(\theta)$ defined in Eq.(4.29) into account. Our basic assumption is that the image f is invariant under some unique symmetry τ_{θ_0}, i.e., θ_0 represents the unknown true symmetry parameter. Thus, our estimate of θ_0 is defined as

$$\widehat{\theta}_{\Delta,N} = \arg\min_{\theta} \widehat{M}_N(\theta),$$

where we write $\widehat{\theta}_{\Delta,N}$ to emphasize the dependence of the estimate on the image resolution Δ and the number of Zernike moments N used to obtain the estimate. For such defined estimate we obtain results that characterize the statistical accuracy of $\widehat{\theta}_{\Delta,N}$. This includes the rate at which $\widehat{\theta}_{\Delta,N}$ tends to θ_0 and the limit law. The following theorems are specialized to the mirror symmetry parameter estimate that minimizes the score function defined in Eq.(4.29) with respect to $\theta \in [0, \pi)$.

Theorem 2. *Suppose that an image function f is of bounded variation on D. Then for sufficiently large N such that the identifiability condition in Eq.(4.24) holds we have*

$$\widehat{\theta}_{\Delta,N} = \theta_0 + O_P(\Delta),$$

where $O_P(\cdot)$ stands for the convergence in probability.

The obtained rate is the optimal one as it is known [19] that the best rate for parameter estimation is the square root of the sample size. This is the case here since Δ is of order $1/n$ and n^2 is the sample size. Also it is worth noting that our situation does not belong to the standard parameter estimation problem as we estimate θ_0 without any knowledge of the underlying image $f(x, y)$. Such problems are referred to as semiparametric, see [19] for the basic theory of semiparametric inference. Furthermore, the selection of N is not critical as we only need N that should define the uniqueness property described in Theorem 1. This should be contrasted with the choice of N for image reconstruction, see Eq.(4.16) and Eq.(4.17).

Next, we establish asymptotic normality for $\widehat{\theta}_{\Delta,N}$. This requires a more restrictive class of image functions.

Theorem 3. *Let the conditions of Theorem 2 be satisfied. Suppose that f is Lipschitz continuous. Then, we have*

$$\Delta^{-1}(\widehat{\theta}_{\Delta,N} - \theta_0) \xrightarrow{\mathcal{L}} \mathcal{N}\left(0, \frac{8\sigma_\varepsilon^2}{M_N^{(2)}(\theta_0)}\right),$$

where

$$M_N^{(2)}(\theta_0) = 8 \sum_{p=0}^{N} \lambda_p^{-1} \sum_{|q| \leq p} q^2 |A_{pq}|^2 \tag{4.30}$$

is the second derivative of $M_N(\theta)$ at $\theta = \theta_0$ and $\mathcal{N}(0, \sigma^2)$ denotes the normal law with mean zero and variance σ^2.

The proofs of Theorem 2 and Theorem 3 can be derived from the results established in [3, 4].

Theorem 3 can be used to construct a confidence interval for θ_0. To this end, we need an estimate of the asymptotic variance in the above normal limit. First, we can estimate $M_N^{(2)}(\theta_0)$ directly by using Eq.(4.30) simply by replacing $A_{pq}(f)$ by $\widehat{A}_{pq}$. Call

this estimate $\widehat{M}_N^{(2)}$. Further, we can estimate the noise variance σ_ε^2 by

$$\hat{\sigma}_\varepsilon^2 = \frac{1}{C(\Delta)} \sum_{(x_i,y_j)\in D} \frac{1}{4}\Big(\big(Z_{i,j} - Z_{i+1,j}\big)^2 + \big(Z_{i,j} - Z_{i,j+1}\big)^2 \Big), \tag{4.31}$$

where the sum is taken over all $(x_i, y_j) \in D$ such that $(x_{i+1}, y_j) \in D$ and $(x_i, y_{j+1}) \in D$, and $C(\Delta)$ is the number of terms in this restricted sum. One can show that if f is Lipschitz continuous, then $\hat{\sigma}_\varepsilon^2 - \sigma_\varepsilon^2 = O_P\big(\Delta\big)$. Using these estimates, we obtain the following confidence interval with nominal level α for θ_0

$$\Big[\widehat{\theta}_{\Delta,N} - q_{1-\alpha}\cdot\frac{2\sqrt{2}\hat{\sigma}_\varepsilon\Delta}{(\widehat{M}_N^{(2)})^{1/2}},\ \widehat{\theta}_{\Delta,N} + q_{1-\alpha}\cdot\frac{2\sqrt{2}\hat{\sigma}_\varepsilon\Delta}{(\widehat{M}_N^{(2)})^{1/2}}\Big], \tag{4.32}$$

where $q_{1-\alpha}$ is the $1-\alpha$-quantile of the standard normal distribution.

Remark 1. If in Theorem 3 we only assume that the image f is a function of bounded variation, then the bias is also of order Δ, and we get an asymptotic offset, i.e., the limiting normal law with non-zero mean.

Remark 2. If the image f is not reflection invariant, the estimator $\widehat{\theta}_{\Delta,N}$ may still converge to a certain parameter value θ^*, which is determined by minimizing the L_2-distance $\|f - \tau_\theta^m f\|^2$. Then $\widetilde{f} = (f + \tau_{\theta^*}^m f)/2$ is the best reflection-symmetric approximation (in the L_2 sense) to the original image f. The following empirical version of $\tilde{f}$

$$\widetilde{f}_N(x,y) = \frac{\widehat{f}_N(x,y) + \tau^m_{\widehat{\theta}_{\Delta,N}}\widehat{f}_N(x,y)}{2}$$

can serve as an estimate of the optimal symmetric version of f. Furthermore, the distance $\|\widehat{f}_N - \widetilde{f}_N\|$ can be used to form an empirical measure of the degree of symmetry of non-symmetric f.

Remark 3. Suppose that f is reflection invariant but is also invariant under some rotation. If f is rotationally invariant, then there will be a minimal angle $\alpha = 2\pi/d$ for some integer d, under which f is rotationally invariant. If we use the estimator $\widehat{\theta}_{\Delta,N}$ in such a situation, then one reflection axis will be between 0 and α, and we should use the minimizer of $\widehat{M}_N(\theta)$ in the interval $[0, \alpha)$ rather than in $[0, \pi)$.

To illustrate the above asymptotic theory let us consider a simple example. Figure 4.3a shows the noisy version of the mirror symmetric image of the resolution 50×50. In Fig.(4.3b) the true contrast functions $M_N(\theta)$ and its estimate $\widehat{M}_N(\theta)$ for $N = 7$ are depicted. A global minimum of $\widehat{M}_N(\theta)$ defines the estimate $\widehat{\theta}_{\Delta,N}$.

Figure 4.4a shows the noisy version of the image being not reflection symmetric. In Fig.(4.4b) the contrast functions $M_N(\theta)$ and $\widehat{M}_N(\theta)$ for $N = 7$ are depicted. The minimum of $\widehat{M}_N(\theta)$ gives the reflection axis angle $\widehat{\theta}_{\Delta,N}$ that defines an estimate of the best symmetric approximation of the image. This optimal symmetric image is estimated by $(\widehat{f}_N + \tau^m_{\widehat{\theta}_{\Delta,N}}\widehat{f}_N)/2$ and is shown in Fig.(4.4c), see Remark 2. In turn, in

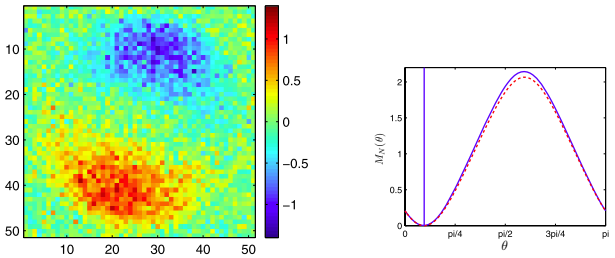

(a) (b)

Figure 4.3: (a) Reflection symmetric noisy image, (b) The contrast functions $M_N(\theta)$ (solid curve) and $\widehat{M}_N(\theta)$ (dashed line) for $N = 7$.

Fig.(4.5) we show the true (in black) and estimated (in red) axes of mirror symmetry of the image depicted in Fig.(4.1).

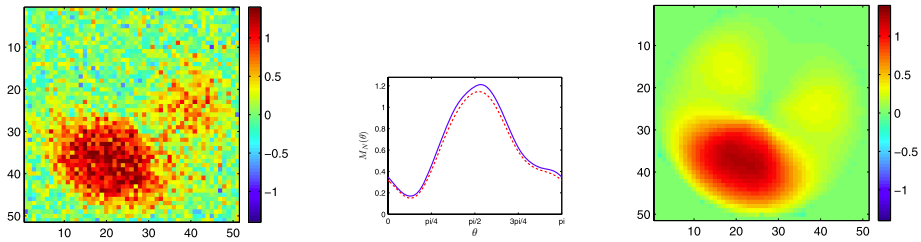

(a) (b) (c)

Figure 4.4: (a) A noisy image that is not reflection symmetric, (b) The contrast functions $M_N(\theta)$ (solid curve) and $\widehat{M}_N(\theta)$ (dashed line) for $N = 7$, (c) An estimate of the best symmetric approximation of the image.

4.4 Symmetry Detection

The aforementioned estimation problem assumes that the image f is invariant under some unique known symmetry, i.e., that there is $\theta_0 \in \Theta$ such that $f = \tau_{\theta_0} f$. In the detection problem our goal is to test the hypothesis on the symmetry class, i.e., we wish to verify

$$H_0 : f = \tau_{\theta_0} f \tag{4.33}$$

for some $\theta_0 \in \Theta$, against the alternative

$$H_a : f \neq \tau_{\theta} f \tag{4.34}$$

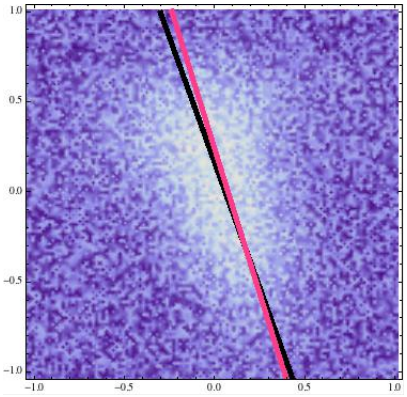

Figure 4.5: The true (in black) and estimated (in red) axes of mirror symmetry of the image depicted in Fig.(4.1)

for all $\theta \in \Theta$. The test statistic for verifying H_0 is based again on the concept of the L_2 minimum distance principle and has the generic form

$$T_N(\Delta) = \| \widehat{f}_N - \tau_{\widehat{\theta}_{\Delta,N}} \widehat{f}_N \|^2, \tag{4.35}$$

where $\widehat{\theta}_{\Delta,N}$ is the above introduced estimate obtained under the null hypothesis H_0. The minimum distance property of $\widehat{\theta}_{\Delta,N}$ suggests the alternative form of T_N, i.e.,

$$T_N(\Delta) = \min_{\theta \in \Theta} \| \widehat{f}_N - \tau_\theta \widehat{f}_N \|^2 . \tag{4.36}$$

This statistic only needs the numerical minimization with respect to a single variable θ. The examined detectors are of the form: reject H_0 if $T_N(\Delta) > c$, where c is a constant controlling the false rejection rate.

Let us begin with the problem of testing the hypothesis of mirror symmetry. Since the minimum L_2-distance approach is invariant for the true value of the reflection angle θ_0 we may consider, without loss of generality, the vertical reflection $\tau^m_{\pi/2} f(x,y) = f(-x,y)$. We will denote this symmetry briefly as $\tau f = f$. In view of Eq.(4.18) we have $A_{pq}(\tau f) = (-1)^{|q|} A^*_{pq}(f)$. Now consider the hypothesis that f is invariant under τ, i.e., $H_0 : f = \tau f$ which can be expressed in terms of Zernike coefficients as $A_{pq}(f) = (-1)^{|q|} A^*_{pq}(f)$. Hence, due to Parseval's formula the test statistic defined in Eq.(4.35) is given by

$$T_N(\Delta) = \sum_{p=0}^{N} \sum_{q=-p}^{p} \lambda_p^{-1} \left| \widehat{A}_{pq} - (-1)^{|q|} \widehat{A}^*_{pq} \right|^2 .$$

The following result presents the limit law for statistic $T_N(\Delta)$ under the hypothesis H_0 as well as under fixed alternatives. Let $C^2(D)$ denote a class of functions possessing two continuous derivatives on D.

Theorem 4. *Under the hypothesis* $H_0 : f = \tau f$, *if* $\Delta \to 0$, $N \to \infty$ *such that* $\Delta N^7 \to 0$, *we have*

$$\frac{T_N(\Delta) - \sigma_\varepsilon^2 \Delta^2 a(N)}{\Delta^2 \sqrt{a(N)}} \xrightarrow{\mathcal{L}} \mathcal{N}(0, 8\,\sigma_\varepsilon^4), \tag{4.37}$$

where $a(N) = (N+1)(N+2)$.
Under a fixed alternative $H_a : f \neq \tau f$, *suppose that* $f \in C^2(D)$. *If* $\Delta N^5 \to \infty$ *and* $N^{3/2}\Delta^{\gamma-1} \to 0$, *where* $\gamma = 285/208$ *controls the geometric error [17], we have*

$$\Delta^{-1}\big(T_N(\Delta) - \|f - \tau f\|^2\big) \xrightarrow{\mathcal{L}} \mathcal{N}(0, 16\sigma_\varepsilon^2 \|f - \tau f\|^2). \tag{4.38}$$

It is worth noting that different rates appear under the hypothesis (fast rate) in Eq.(4.37) and under fixed alternatives (slow rate) in Eq.(4.38). This takes place since $T_N(\Delta)$ is (under the hypothesis) a quadratic statistic [5], but under a fixed alternative an additional linear term arises which dominates the asymptotic. Theorem 4 can be used to construct an asymptotic level α test for verifying the hypothesis H_0. Indeed, fixing the Type I detection probability $P\{T_N(\Delta) > c|H_0\}$ to the value α yields the following asymptotic choice of the control limit c

$$c_\alpha = 2q_{1-\alpha}\Delta^2\sqrt{2a(N)}\hat{\sigma}_\varepsilon^2 + \Delta^2 a(N)\hat{\sigma}_\varepsilon^2,$$

where $\hat{\sigma}_\varepsilon^2$ is an estimate of σ_ε^2, see Eq.(4.31) and the truncation parameter N can be specified as $N = \Delta^{-\alpha}$, where $0 < \alpha < 1/7$. Hence, H_0 is rejected if $T_N(\Delta) > c_\alpha$.

The result of Theorem 4 also reveals that under the alternative

$$T_N(\Delta) \to \| f - \tau f \|^2 \quad (P) \tag{4.39}$$

as $\Delta \to 0$. Consequently, we readily obtain that $N^5 \Delta T_N(\Delta) \to \infty$ (P) which implies the following consistency result.

Theorem 5. *Let* $H_a : f \neq \tau f$ *for* $f \in C^2(D)$ *hold. If* $\Delta N^5 \to \infty$ *and* $N^{3/2}\Delta^{\gamma-1} \to 0$, *then as* $\Delta \to 0$

$$P\left\{N^5 \Delta T_N(\Delta) > c|H_a\right\} \to 1 \tag{4.40}$$

for any positive constant $c > 0$.

Hence, the properly normalized decision statistic $T_N(\Delta)$ leads to the testing technique that is able to detect that the null hypothesis is false with the probability approaching to one, i.e., the power of the test tends to one.

Furthermore, let us note that contrary to the symmetry estimation problem the symmetry detection requires the optimal choice of the truncation parameter N. The condition $\Delta N^7 \to 0$, used under the hypothesis, is rather restrictive, and is due to the only approximate orthogonality of the discretized Zernike polynomials. This condition can be relaxed if we assume a more accurate orthogonal design. In fact, if we have exact discrete orthogonality, then $\Delta N^2 \to 0$ is sufficient for Eq.(4.37) to hold. Under a fixed alternative, the condition $N^{3/2}\Delta^{\gamma-1} \to 0$ is equivalent to $N^{4+\beta}\Delta \to 0$, $\beta = 0.0519\ldots$, so that this condition and $N^5\Delta \to \infty$ can be fulfilled simultaneously.

Analogous derivations can be carried out for testing d-fold rotation symmetry. Explicit results can be obtained for $d = 2$ and $d = 4$. The remaining cases need some interpolation procedures since the discrete grid points $\{(x_i, y_j)\}$ are no longer invariant under $\tau^r_{2\pi/d}$ for arbitrary value of d.

To illustrate this case let us consider an example of the 2-fold rotation symmetric image f_1 shown in Fig.(4.6) (top row). The second row in Fig.(4.6) depicts the reconstruction $\widehat{f}_N$ and the corresponding error image $\widehat{f}_N - f_1$. The reconstruction $\widehat{f}_N$ here is based on the complete Zernike function expansion that ignores the fact that the image was detected to be symmetric. On the other hand, the third row in Fig.(4.6) shows the reconstruction $\widehat{f}^r_N$ and the error $\widehat{f}^r_N - f_1$ that takes into account the existing symmetry of f_1. In fact, under the 2-fold rotation symmetry we have that the Zernike moments $A_{pq} = 0$ for all q being odd. Hence, the reconstruction $\widehat{f}^r_N$ shown in the third row of Fig.(4.6) is using only Zernike functions with even q. It is seen that both reconstructions reveal comparable errors, with the preferable visual quality of the symmetry preserving reconstruction $\widehat{f}^r_N$.

Analogous experiments have been repeated for the not 2-fold rotation symmetric image f_2 depicted in the top panel of Fig.(4.7). The second row of Fig.(4.7) shows the full Zernike function reconstruction $\widehat{f}_N$ and the corresponding error image $\widehat{f}_N - f_2$. On the other hand, the third row in Fig.(4.7) shows the reconstruction $\widehat{f}^r_N$ and the error $\widehat{f}^r_N - f_2$ that falsely assumes that f_2 is 2-fold rotation symmetric. The dramatic increase of the reconstruction error is clearly seen. Hence, either accepting or rejecting the hypothesis of the image symmetry has an important influence on its visual perception and recognition.

The case $d = \infty$ (testing radiality) is of special interest and can be examined by observing that if the image f is radial, i.e., $f(\rho, \varphi) = g(\rho)$, then we have that $A_{pq}(f) = 0$ for all $q \neq 0$. Moreover,

$$A_{p0}(f) = 2\pi \int_0^1 g(\rho) P_{p/2}(2\rho^2 - 1)\rho d\rho,$$

where $P_s(x)$ is the Legendre polynomial of order s. This allows us to form the appropriate nonparametric test for the image radiality with the power tending to one as $\Delta \to 0$, see [16].

It is rare in practise to pose a null hypothesis that the verified not observed image is exactly symmetric. Thus, the exact symmetry hypothesis is replaced by the following approximate symmetry requirement

$$H^\delta_0 : \|f - \tau_{\theta_0} f\| \leq \delta \tag{4.41}$$

with the alternative hypothesis as

$$H^\delta_a : \|f - \tau_{\theta_0} f\| > \delta, \tag{4.42}$$

where δ is the assumed degree of image symmetry. This type of hypothesis can be incorporated into our previous scheme by rejecting H^δ_0 if $T_N(\Delta) - \delta > c_\alpha$.

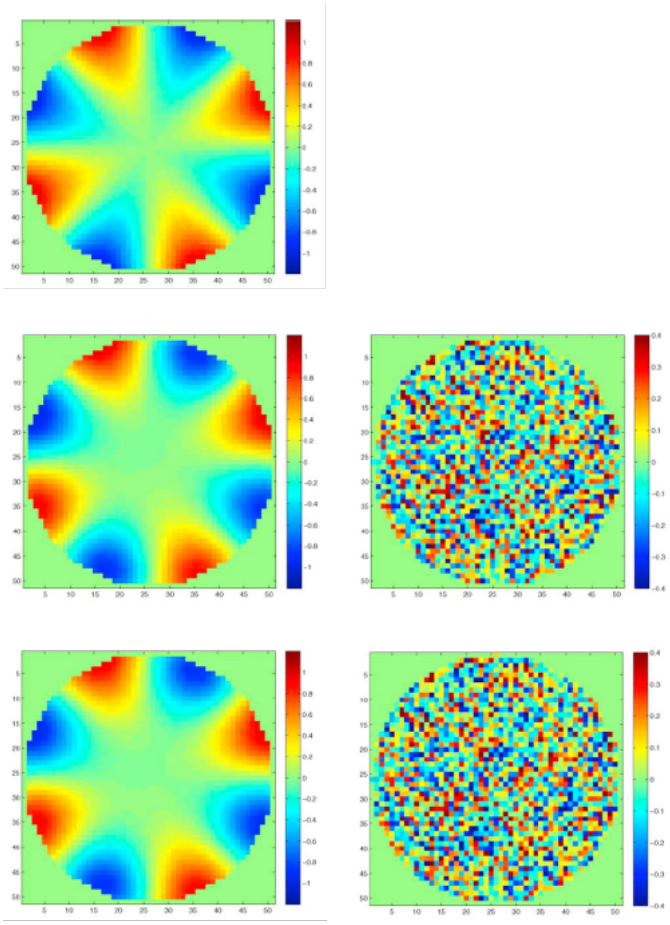

Figure 4.6: The 2-fold rotation symmetric image f_1 (top panel). The full Zernike function reconstruction $\widehat{f}_N$ and the error image $\widehat{f}_N - f_1$ (second panel). The reconstruction $\widehat{f}_N^r$ and the error $\widehat{f}_N^r - f_1$ that takes into account the existing symmetry of f_1 (third panel).

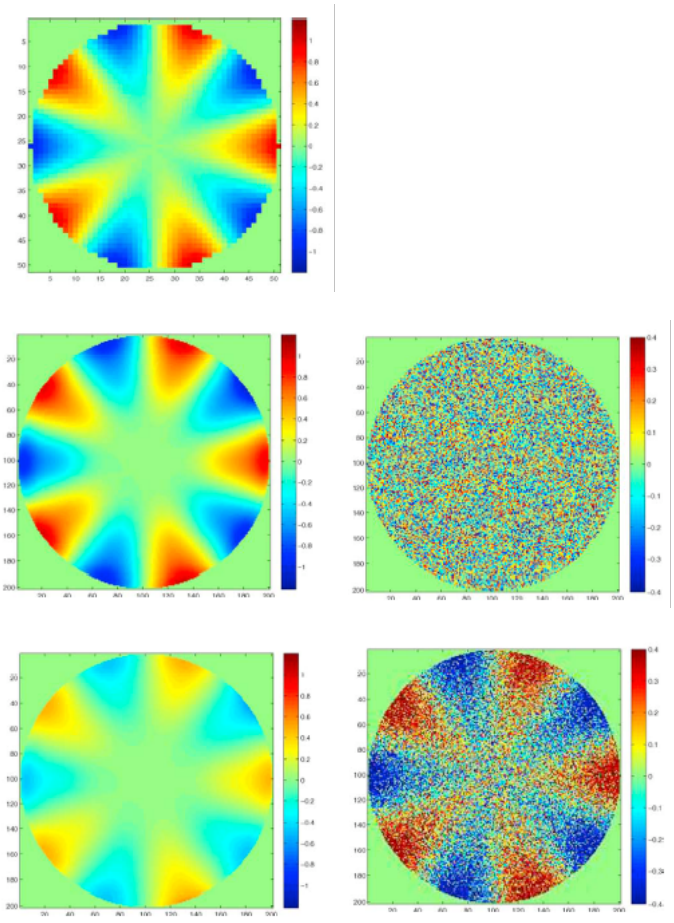

Figure 4.7: The image f_2 that is not 2-fold rotation symmetric (top panel). The full Zernike function reconstruction $\widehat{f}_N$ and the error image $\widehat{f}_N - f_2$ (second panel). The reconstruction $\widehat{f}^r_N$ and the error $\widehat{f}^r_N - f_2$ that uses the symmetry assumption (third panel).

4.5 Concluding Remarks

In this chapter, we give the unified minimum L_2-distance radial moments based approach for statistical assessing the image symmetry. The problem of symmetry estimation can be regarded as a semiparametric estimation problem, with θ as the target parameter, and the image function as a nonparametric nuisance component [19]. Further results may include the statistical assessment of imperfect symmetries, symmetries that only hold locally and detection and estimation of joint symmetries. In particular, the problem of detection and estimation of symmetry for blurred images is of the great interest, i.e., when the observation model in Eq.(4.5) is replaced by

$$Z_{i,j} = \iint_D K(x_i - x, y_j - y) f(x, y) dx dy + \varepsilon_{i,j},$$

where $K(x, y)$ is the point-spread function of the given imaging system. Such a case plays important role in confocal microscopy and medical imaging [3, 4].

Further extensions may also include 3-D imaging where a number of basic symmetry classes is much larger than in the 2-D case.

References

[1] A.B. Bhatia and E. Wolf. On the circle polynomials of Zernike and related orthogonal sets. In *Mathematical Proceedings of the Cambridge Philosophical Society*, volume 50, 1954.

[2] M. Birke, H. Dette, and K. Stahljans. Testing symmetry of nonparametric bivariate regression function. *Journal of Nonparametric Statistics*, 23(2):547–565, 2011.

[3] N. Bissantz, H. Holzmann, and M. Pawlak. Testing for image symmetries-with application to confocal microscopy. *IEEE Transactions on Information Theory*, 55(4):1841–1855, 2009.

[4] N. Bissantz, H. Holzmann, and M. Pawlak. Improving PSF calibration in confocal microscopic imaging - estimating and exploiting bilateral symmetry. *Annals of Applied Statistics*, 4(4):1871–1891, 2010.

[5] P. de Jong. A central limit theorem for generalized quadratic forms. *Probability Theory and Related Fields*, 75(2):261–277, 1987.

[6] S. Derrode and F. Ghorbel. Shape analysis and symmetry detection in gray-level objects using the analytical Fourier-Mellin representation. *Signal Processing*, 84(1):25–39, 2004.

[7] J. Flusser, T. Suk, and B. Zitova. *Moments and Moment Invariants in Pattern Recognition*. Wiley, Chichester, 2009.

[8] Y. Keller and Y. Shkolnisky. A signal processing approach to symmetry detection. *IEEE Transactions on Image Processing*, 15(8):2198–2207, 2006.

[9] W.Y. Kim and Y.S. Kim. Robust rotation angle estimator. *IEEE Transactions on Pattern Analysis and Machine Intelligence*, 21(8):768–773, 1999.

[10] S.X. Liao and M. Pawlak. On the accuracy of Zernike moments for image analysis. *IEEE Transactions on Pattern Analysis and Machine Intelligence*, 20(12):1358–1364, 1998.

[11] Y. Liu, H. Hel-Or, C.S. Kaplan, and L. van Gool. *Computational Symmetry in Computer Vision and Computer Graphics*. Now Publishers, Boston, 2010.

[12] G. Loy and A. Zelinsky. Fast radial symmetry for detecting points of interest. *IEEE Transactions on Pattern Analysis and Machine Intelligence*, 25(8):959–973, 2003.

[13] L. Lucchese. Frequency domain classification of cyclic and dihedral symmetries of finite 2-d patterns. *Pattern Recognition*, 37(12):2263–2280, 2004.

[14] G. Marola. On the detection of the axes of symmetry of symmetric and almost symmetric planar images. *IEEE Transactions on Pattern Analysis and Machine Intelligence*, 11(1):104–108, 1989.

[15] R. Mukundan and K.R. Ramakrishnan. *Moment Functions in Image Analysis: Theory and Appplications*. World Scientific, Singapore, 1998.

[16] M. Pawlak. *Image Analysis by Moments: Reconstruction and Computational Aspects*. Wroclaw University of Technology Press, Wroclaw, 2006. http://www.dbc.wroc.pl/dlibra/doccontent?id=1432&from=&dirids=1.

[17] M. Pawlak and S.X. Liao. On the recovery of a function on a circular domain. *IEEE Transactions on Information Theory*, 48(10):2736–2753, 2002.

[18] J. Rosen. *Symmetry in Science: An Introduction to the General Theory*. Springer-Verlag, New York, 1995.

[19] A. W. van der Vaart. *Asymptotic Statistics*. Cambridge University Press, Cambridge, 1998.

[20] Q. Wang, O. Ronneberger, and H. Burkhardt. Rotational invariance based on Fourier analysis in polar and spherical coordinates. *IEEE Transactions on Pattern Analysis and Machine Intelligence*, 31(9):1715–1722, 2009.